
Article:
Wang, B., Wang, J., Griffo, A. orcid.org/0000-0001-5642-2921 et al. (1 more author) (2019) Experimental assessments of a triple redundant 9-phase fault tolerant PMA SynRM drive. IEEE Transactions on Industrial Electronics, 66 (1). pp. 772-783. ISSN 0278-0046

https://doi.org/10.1109/TIE.2017.2784368

Experimental Assessments of a Triple Redundant 9-Phase Fault Tolerant PMA SynRM Drive

Bo Wang, *Member IEEE*, Jiabin Wang, *Senior Member, IEEE*, Antonio Griffo, *Member IEEE*, Bhaskar Sen, *Member IEEE*

***Abstract*—Fault tolerant machine drives are key enabling technologies in safety critical applications. The machine drives are expected to exhibit high performance in healthy conditions and accommodate as many faults as possible, namely open circuit or short circuit in the machine and inverter or even an inter-turn short circuit. This paper aims to assess a triple redundant 9-phase (3x3-phase) permanent magnet assisted synchronous reluctance machine (PMA SynRM) drive by comprehensive experimental tests under both healthy and fault conditions on a 35kW machine drive prototype. The healthy performance, fault behavior, fault detection and mitigation strategy are presented and assessed by extensive tests which demonstrate that the machine drive exhibits high performance and excellent fault tolerance with simple and cost-effective implementation. Therefore, the proposed machine drive has proven to be a practical candidate for safety critical applications.**

***Index Terms*—Fault tolerant machine, Fault tolerant drive, permanent magnet machine, synchronous reluctance machine, experimental test, open circuit, short circuit, turn fault, fault detection.**

I. Introduction

FAULT tolerant machine drives are desirable in safety critical applications due to its uninterrupted operation capability under fault conditions [1]. For practical applications, a fault tolerant machine drive is required to exhibit high performance in healthy operation and it is also expected to tolerate or sustain as many faults as possible [2, 3]. However, these two requirements usually conflict with each other [4]. In [5], 3-phase machine has been investigated for post fault operation after open circuit failure in induction machine and permanent magnet (PM) machine respectively. The concept has also been extended to multi-phase machines for increased post fault torque capability and controllability [6, 7]. It should be noted that customized inverters are required which complicate the implementation and control [8, 9]. The machine winding may be configured as multiple 3-phase windings which owns the multiple electrical ports feature and facilitates the fast integration of standard 3-phase inverters.

In order to accommodate inter-turn short circuit fault in machines, fractional slot concentrated winding (FSCW) machine [10] and switched flux PM machine [11] have been modified by adopting special design in the slot geometry to increase the self-inductance. Although these measures could improve fault tolerance, they also have negative impact on the machine performance, such as increased size and cost, reduced torque density and efficiency.

PM machines are featured as high efficiency and high torque density, therefore being favored by high performance applications. However, the PM field becomes a disadvantage for fault tolerance since it cannot be turned off in the event of a fault. The PM field could cause excessive fault current in case of an inter-turn short circuit failure even the current excitation has been removed [12]. In addition, the back emf in high speed could be much greater than the DC link voltage which may cause uncontrolled rectification if the inverter fails [13]. Therefore, the PM field should be restricted, but this is in conflicted with torque production in machines which rely on the PM field, such as FSCW PM machines and other surface-mounted PM machines.

While variety of fault tolerant machine drive concepts have been reported in literature, many only deal with less severe open-circuit fault. Cost-effective solutions that can cope with most electric faults, in particular, inter-turn short circuit fault, would be desirable. In [14], a triple redundant 9-phase PMA SynRM drive is proposed and analyzed. It has been shown by simulation that the machine drive exhibits high performance and are capable of tolerating various electric faults. This paper aims to conduct comprehensive experimental tests for the 9-phase PMA SynRM drive to examine its performance in healthy conditions, machine behavior in typical fault conditions and its ability to tolerate these faults [15]. Detailed experimental

Manuscript received July 28, 2017; revised September 24, 2017 and November 3, 2017; accepted November 23, 2017.

The authors are with the Department of Electronic and Electrical engineering, The University of Sheffield, Sheffield, S1 3JD United Kingdom (e-mail: bowing.ee@hotmail.com; j.b.wang@sheffield.ac.uk; a.griffo@sheffield.ac.uk; bsen.ee@gmail.com).

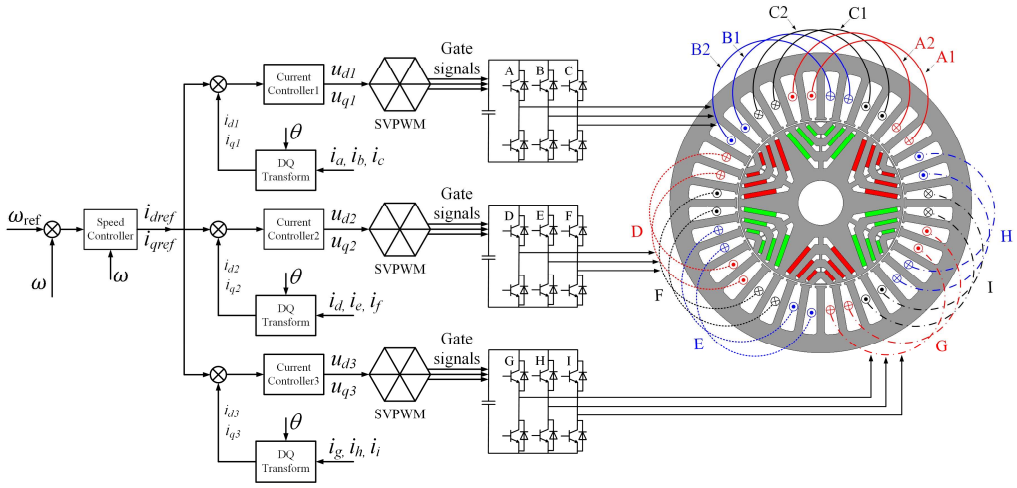

Fig. 1. Triple redundant 9-phase PMA SynRM drive.

results and analysis demonstrate that the machine exhibits comparable performance to conventional PM machine, while it provides enhanced fault tolerance for various faults, including single turn short circuit in the worst case. And the fault tolerant properties are realized in a simple and cost effective manner, making it as an ideal candidate for fault tolerant applications.

II. Triple Redundant 9-Phase PMA SynRM Drive

The machine under consideration is a 36-slot 6-pole PMA SynRM as shown in Fig. 1 [14]. PMA SynRM is well known for its hybrid torque production mechanism which is a combination of PM torque and reluctance torque [16]. The reluctance torque enables less use of magnets without decreasing the torque capability, therefore exhibiting comparable performance with conventional PM machines. The low PM field reduces the fault current in case of a short circuit fault. It also eliminates the possibility of uncontrolled generation at high speed, therefore enhancing the fault tolerance of the machine.

The conventional overlapped distributed winding is reconfigured as triple 3-phase non-overlapped windings with each driven by a standard 3-phase inverter. Due to the segregated windings and independent drives, physical, electrical and thermal isolations are obtained between the three 3-phase sets. The three inverter drive modules share the same current references from the speed controller but track them by independent current controllers in *dq* frame. For this configuration, a failure in one 3-phase set does not significantly affect the operation of other two 3-phase sets. Hence, the risk of fault propagation between different 3-phase winding sets is minimized, providing tolerance to various faults [2]. Since only the conventional overlapped windings are rearranged, the merits of PMA SynRM, such as reduced magnet usage, low back emf, inherent large reluctance torque, high efficiency and high torque density are maintained. Further, the multiple 3-phase winding configuration facilitates the application of standard 3-phase inverters with the same VA rating as one single 3-phase inverter configuration. Therefore, the overall cost is nearly the same as one 3-phase inverter while the heat can be spread more evenly to the three inverter modules [17].

Table I
MACHINE SPECIFICATIONS

Specification	Symbol	Value
Base speed	n_b	4000rpm
Maximum speed	n_m	19200rpm
Rated power	P_r	35kW
Rated current	I_{rated}	120A
Nominal DC link voltage	V_{dc}	270V
Cooling medium		Aeroshell oil

Table II
LEADING GEOMETRY PARAMETERS

Parameter	Symbol	Value
Stator radius	R_s	90mm
Back iron thickness	H_j	10.25mm
Tooth width	T_w	5.1mm
Rotor radius	R_l	51.75mm
Shaft radius	R_s	13.5mm
Axial stack length	L_a	110mm
Turn number of each coil	N	8

If an open-circuit fault occurs in an inverter switch or winding, the faulty 3-phase winding set can be simply deactivated by opening all the switches in that set, the remaining two healthy sets can continue operation to provide torque. In case of a short circuit failure, terminal short circuit (TSC) can be applied to the faulty set by closing all three bottom or top switches of the corresponding 3-phase inverter. Due to the low PM field, the resultant short circuit currents are limited below the rated value. In the worst case when an inter-turn short circuit fault occurs, the current of the fault turns can be reduced by applying TSC to nullify the flux in the fault region. If the three inverters are supplied from three independent DC sources, the proposed drive system has three independent electrical ports and can tolerate DC supply fault and DC-link capacitor fault. Thus, owing to the triple redundancy, a fault in one 3-phase system can be isolated and the other two 3-phase sets can continue operation to deliver torque or power.

In order to experimentally assess the machine performance under both healthy and fault conditions, a prototype machine has been built as shown in Fig. 2. The machine specification and leading geometry parameters are given in Table I and Table

II, respectively. The stator stack is skewed by one slot, i.e. 10 degree to reduce the torque ripple and voltage harmonics due to slotting, as shown in Fig. 2(a). The rotor stack is shown in Fig. 2(b), in which the magnets have been inserted in the cavity. Epoxy has been injected to the void area to protect the magnets and improve thermal dissipation. The key feature of the fault tolerant machine is the segregated windings as shown in Fig. 2(c). It can be seen that the windings of different 3-phase sets have been separated by the proposed winding configuration. Insulation paper is inserted between different phases to enhance the phase-to-phase insulation. The windings are further protected by Stycast potting to improve the thermal dissipation in the slots and end windings as shown in Fig. 2(d). Circular grooves are embedded in the stator housing surface to facilitate oil cooling as shown in Fig. 2(e). The final machine assembly with the oil inlet and outlet is shown in Fig. 2(f). Thermocouples have been buried in the slots and end windings to monitor the winding temperatures.

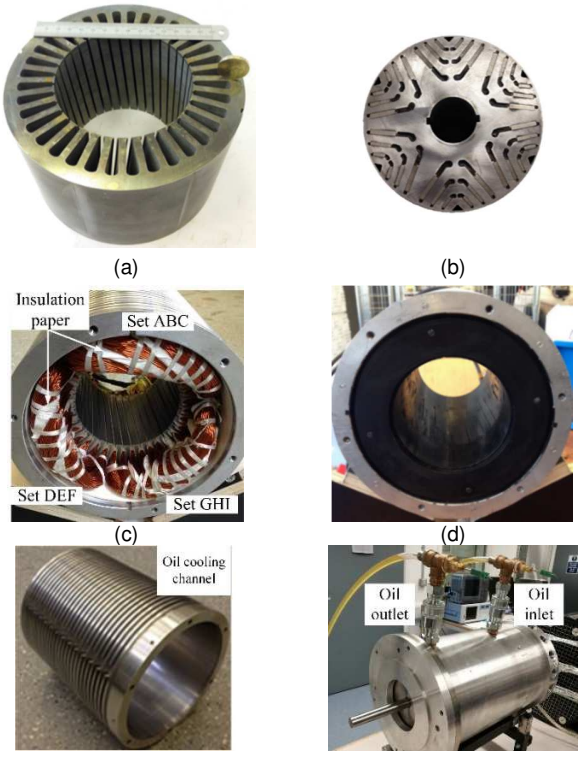

Fig. 2. Machine prototype (a) Skewed stator stack (b) Rotor stack with magnets (c) Segregated windings (d) Stycast potted stator (e) Oil cooling jacket (f) Machine assembly.

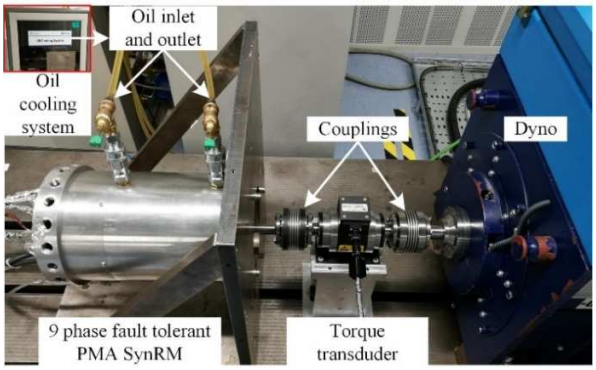

Fig. 3. 9-phase PMA SynRM test rig.

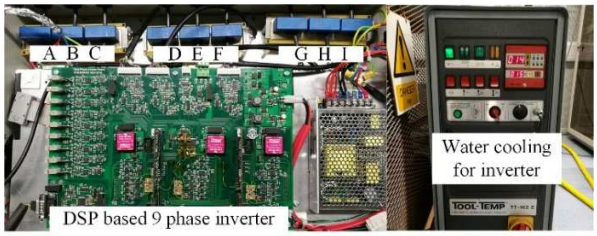

Fig. 4. DSP based 9-phase inverter.

The integrated test rig is shown in Fig. 3. The machine is connected to a dyno via two couplings with an inline torque transducer. During tests, the dyno operates in speed mode while the machine drive under study operates in torque mode. It is controlled by a DSP based 9-phase inverter, consisting of three standard 3-phase inverters as shown in Fig. 4. An oil pump and a water pump have been implemented for the machine and inverter liquid cooling, respectively. During tests, the 9 phase currents are measured by current sensors and the data are stored in the DSP RAM. Tests of the prototype machine drive are first performed under healthy conditions, such as measurements of the back emf, no load loss, characteristic current, maximum torque per ampere (MTPA) point and efficiency. Then, the machine drive is tested in various fault conditions to assess its fault tolerance, including the open circuit, short circuit and single turn short circuit fault. Fault detection and fault mitigation also have been implemented and tested in the drive. Thermal tests are performed under the rated conditions considering the worst case of single turn short circuit condition to record the temperature rise.

III. Test Under Healthy Condition

A. Back Emf Test

First, the phase back emfs of set ABC are measured at base speed 4000rpm as shown in Fig. 5. This is made possible from a neutral point lead in ABC set. Due to stator skew, the back emfs are virtually free from tooth ripple harmonics. Since the machine is configured as triple 3-phase sets, symmetry between the three sets is examined as shown in Fig. 6. The line-to-line back emfs of the three sets essentially coincide with each other, confirming good symmetry between them.

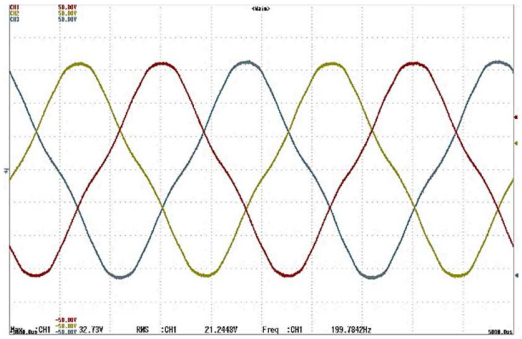

Fig. 5. Phase back emf waveform at 4000rpm, *x*-axis, 1ms/div, *y*-axis, 10V/div, red, U_A, yellow, U_B, blue, U_C.

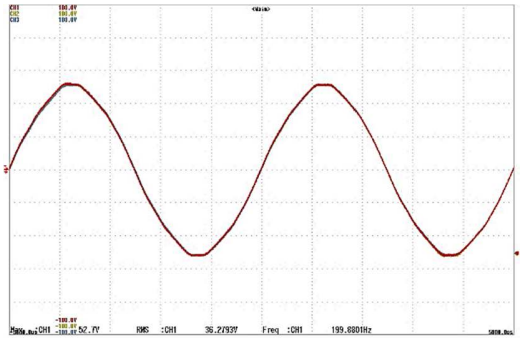

Fig. 6. Line-to-line back emf waveform at 4000rpm, *x*-axis, 1ms/div, *y*-axis, 20V/div, red, U_{AB}, yellow, U_{DE}, blue, U_{GH}.

The back emfs are measured at several different speeds up to 12000rpm. Linearity is observed and it can be deduced from the results that the peak line-to-line back emf at the maximum speed 19200rpm is 246.5V which is lower than the DC link voltage 270V. Therefore, uncontrolled rectifier generation will not take place even if the inverter fails. This fail-safe feature is desirable for the PM machine drives which require to operate in high speed region.

B. Characteristic Current Measurement

The characteristic current I_{ch} is expressed by (1) where φ_m is the phase PM flux linkage and L_d is the *d*-axis inductance for each 3-phase set. It can be measured by short circuiting all three 3-phase sets.

$$I_{ch} = \varphi_m / L_d \tag{1}$$

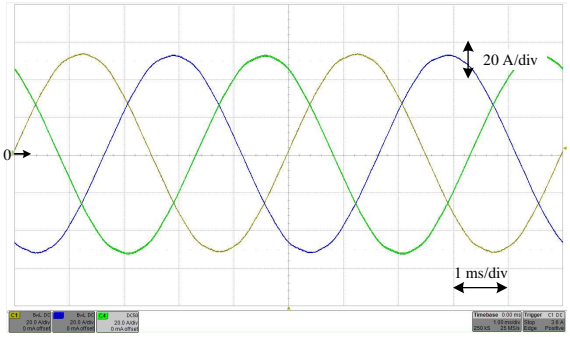

Fig. 7. Phase currents of set ABC at 4000rpm with three 3-phase sets short circuited, yellow, i_A, blue, i_B, green, i_C.

The measured characteristic currents at 4000rpm are shown in Fig. 7. As will be seen, the peak current is only 53.6A which is lower than half of the rated current. The low characteristic current is mainly due to the low PM field. The TSC currents do not cause any thermal risk to the machine and, therefore, TSC in one 3-phase set can be employed as a mitigation action in case of a short circuit fault in that set.

C. No load Loss Measurement

The no load loss mainly consists of iron loss and mechanical loss. The iron loss includes the loss in lamination and magnets while the mechanical loss is due to the bearing loss and windage loss.

The no load loss of the prototype machine is measured by a precision torque transducer as shown in Fig. 8 up to 12000rpm. The mechanical loss can be measured by building a dummy rotor with the same dimension and weight without magnets. However, in this case the mechanical loss is estimated from an existing dummy rotor with similar dimension [18] by using empirical formula in [19] as shown in Fig. 8.

Subtracting the mechanical loss from the no load loss, the no load iron loss can be obtained as shown in Fig. 9. Meanwhile, the iron loss is calculated in finite element analysis according to the manufacture data and the results are also shown in Fig. 9. There is small difference between the predicted and measured iron losses which may be attributed to the manufacture process, machine assembly and limited accuracy of torque transducer. This error can be reduced by multiplying a "built factor". It can be seen that by introducing a built factor of 1.2, the calibrated iron loss is reasonably close with the measured values.

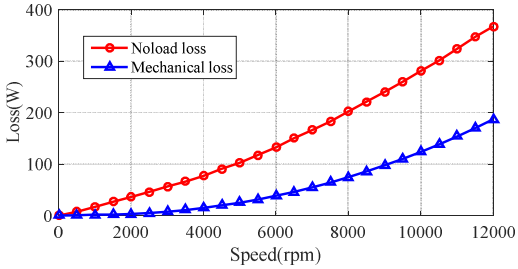

Fig. 8. No load loss and Mechanical loss variations with speed.

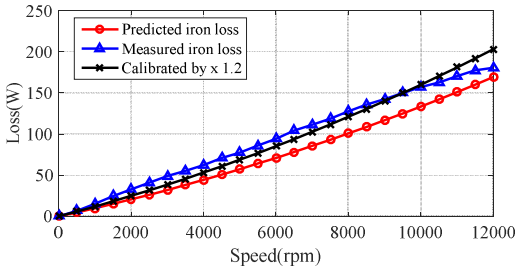

Fig. 9. No load iron loss variations with speed.

D. MTPA Test

Load tests are performed on the prototype drive by current excitation using the three 3-phase inverters. As discussed previously, torque in the PMA SynRM is contributed by both PM torque and reluctance torque. Therefore, MTPA points should be identified for required torque with minimum current. For a given current magnitude, the MTPA point is determined by scanning the current vector angle with respect to the *q*-axis as shown in Fig. 10, denoted as gamma angle γ in a wide range at 500rpm. The measured torque gamma angle loci when the

current magnitude is varied from 20A to 120A is shown in Fig. 11. As can be seen, the optimum gamma angle increases with current magnitude (or load torque). The reluctance torque ratio has been calculated using frozen permeability method as shown in Fig. 12 [20].When the current magnitude is greater than 50% of the rated, the reluctance torque becomes dominant. Thus, even in an unlikely case of partial demagnetization, the machine can still output considerable torque by exploiting the reluctance torque.

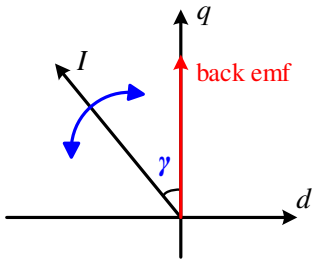

Fig. 10. Illustration of current vector and gamma angle γ.

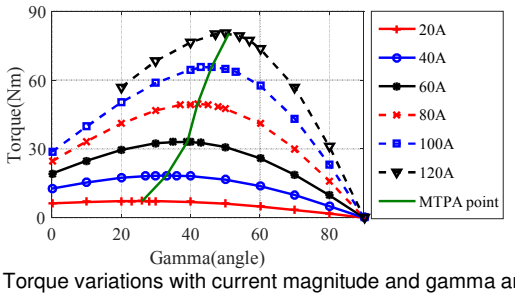

Fig. 11. Torque variations with current magnitude and gamma angle.

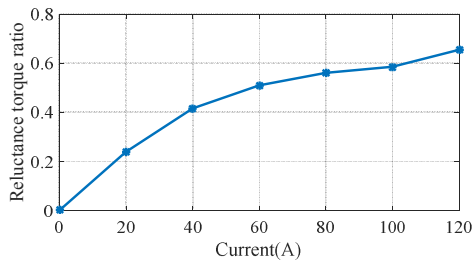

Fig. 12. Reluctance torque ratio against the current magnitude.

E. Efficiency Measurement

The machine efficiency at the base speed of 4000rpm when operating at the MTPA points determined from the previous tests is measured by Yokogawa WT 3000 power analyzer with high bandwidth and precision current and voltage transducers, and in-line torque transducer. Since the power analyzer can only measure the electrical input power for one 3-phase set, the input powers of the three 3-phase sets are measured separately and then added together to obtain the total input power. The efficiency measurement is repeated at the based speed 4000rpm when the current magnitude is varied from 10A to 120A. The resultant efficiency variation with load torque is shown in Fig. 13. It can be seen that the machine efficiency is higher than 95% in most torque range, and the efficiency at the rated operation point is 94.6%. The high efficiency is mainly attributed to the hybrid torque production mechanism in that even with low magnet usage, the machine can achieve high efficiency thanks to considerable reluctance torque contribution.

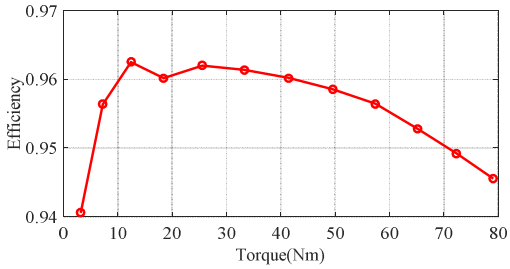

Fig. 13. Efficiency variation with load torque at 4000rpm in healthy condition.

The phase currents of set ABC at 4000rpm are measured by a LeCroy oscilloscope as shown in Fig. 14. The currents are well controlled with small distortion near the peak. Switching harmonics can be seen in the waveforms. Good symmetry is also observed between the three 3-phase sets as shown in Fig. 15, where the data is obtained from the DSP RAM. Due to the limited current probes of the oscilloscope, the 9 phase currents are mainly measured by the inverter current sensors and stored in the DSP RAM, and consequently the switching harmonics are not visible due to limited sampling frequency and anti-alias filtering.

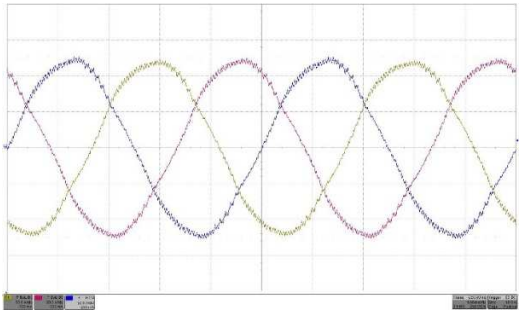

Fig. 14. Phase currents of set ABC at 4000rpm in healthy condition, *x*-axis, 1ms/div, *y*-axis, 50A/div, yellow, i_A, red, i_B, blue, i_C.

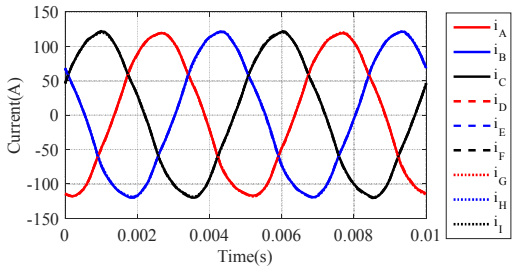

Fig. 15. 9 phase currents at 4000rpm in healthy condition.

F. Thermal Test in Healthy Condition

The machine thermal behavior affects the winding insulation degradation rate and remaining life time. The temperature rise also changes the conductivity of the copper wire considerably which influences the copper loss. Thus, the thermal test is performed by operating the machine drive in healthy condition for 2 hours. The machine is loaded with the rated current 120A at base speed with oil cooling at a flowrate of 7 litre/min. The variations of the temperatures in the oil inlet, oil outlet and windings are recorded by the thermocouples as shown in Fig. 16. Due to the limited capacity of the heat exchanger, the temperatures of the oil inlet and outlet increase from 24°C to 44°C and from 25°C to 57°C, respectively. Since the machine

is operating in healthy condition, the temperature rise of the three 3-phase sets should be similar due to the same load current. It is noticed that the temperatures in the slots, i.e. in B1 slot, E2 slot and B2 slot where a tap for emulation of a single turn short circuit is placed, are quite close. The differences are less than 4 degrees. However, the temperature in set DEF end winding is 11 degrees higher than that of ABC set. This can be attributed to the loss caused by the neutral connection. For set ABC, the neutral is connected outside of the machine for easy access while the neutral of DEF is terminated in the end winding region. The neutral connection is made by soldering the three phase terminals which leads to additional resistance and loss. Since the corresponding thermocouple is placed close to the neutral point of set DEF, a higher temperature rise would be expected in set DEF end winding region. Nevertheless the temperature is far below 200°C for continuous operation of Class C insulation used for the windings.

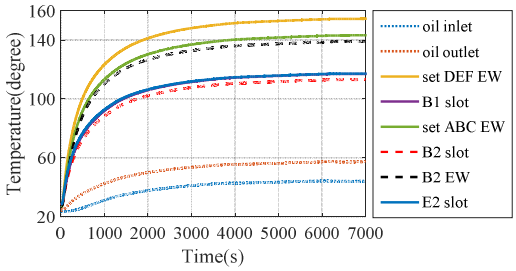

Fig. 16. Thermal test results with 120A at 4000rpm in healthy condition.

IV. Tests Under Fault Conditions

In this section, the machine fault behavior and post fault torque capability are investigated for open circuit, short circuit and inter-turn short circuit fault. The fault tolerant operation of the drive under inter-turn fault is demonstrated including the heathy operation, fault injection, fault detection and fault mitigation. The results are presented and discussed.

A. One 3-phase Set Open Circuit Test

If the switches or windings experience an open circuit fault in one 3-phase set, the fault can be tolerated by just turning off all the gate drivers. Owing to the triple redundancy, the remaining healthy sets can continue operation to provide torque. This one 3-phase set open circuit mode has been tested by deactivating set ABC while exciting sets DEF and GHI at 4000rpm. The load currents vary from 20A to 120A in magnitude and the gamma angles of the current vectors are set to the MTPA points in the healthy condition. The measured post fault torque is compared with that in the healthy condition in Fig. 17. It can be seen that the machine is capable of providing about 2/3 of the torque in healthy condition.

Further, the current waveforms in the two healthy 3-phase sets with 120A excitation are shown in Fig. 18. As can be seen, the phase currents are no longer in a balanced manner, and some distortions are present in both sets. This is because the three 3-phase sets are not magnetically isolated. Thus, when one set is open circuited, the flux-linkages and induced voltages in other two heathy sets are affected due to the magnetic coupling. Consequently, more distortion in current waveforms is seen due to limited control bandwidth.

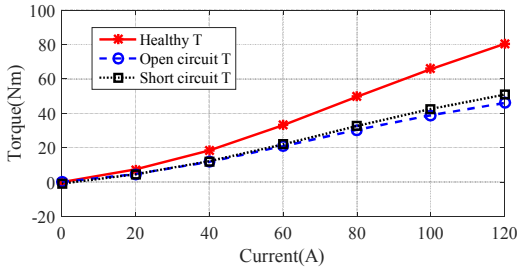

Fig. 17. Variations of torque with currents under healthy, set ABC open circuit and short circuit conditions.

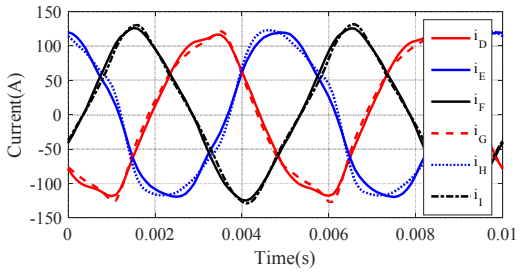

Fig. 18. Healthy phase currents at 4000rpm when set ABC open circuited.

B. One 3-phase Set Short Circuit Test

If a short circuit occurs in the inverter switches or the windings of one 3-phase set, TSC should be applied on the fault set to avoid further damage. The TSC is realized by turning on all three top or bottom switches of the respective inverter or more practically by setting the *d*- and *q*-axis voltage commands to zero in the controller. The one set short circuit mode is tested by short circuiting set ABC while the current excitations in the healthy sets DEF and GHI are varied from 20A to 120A at 4000rpm. The resultant torque variation is shown in Fig. 17 together with those under healthy and open-circuit conditions. The torque capability is slightly higher than that of the open circuit mode. It is noticed that the machine exhibits a small braking torque when the currents in the two healthy sets are zero.

The induced short circuit currents in set ABC when the two healthy sets are excited with 120A currents are shown in Fig. 19. It is seen that the phase currents are highly unbalanced due to the mutual magnetic coupling between the three 3-phase sets. The root-mean-square (RMS) current in phase A is much lower than those in phases B and C. Nevertheless, due to the low PM field, the RMS values of the short circuit currents are much lower than the rated. Hence the machine drive can sustain the short circuit fault without any thermal risk. Fig. 20 shows the phase currents in the healthy 3-phase sets where small unbalance and distortion are also observed.

The torque ripples with the rated current of 120A at 500rpm under healthy, open-circuit and short circuit conditions are measured, and the results are shown in Fig. 21. In healthy condition, the torque waveform is quite flat and torque ripple is low due to the stator skew. In open circuit and short circuit conditions noticeable 2nd harmonics appear which can be attributed to their mutual magnetic coupling and imperfect current excitations in the three 3-phase sets. The torque ripple

is slight higher in open circuit condition and the peak-to-peak variation is 5Nm, or 6% of the rated.

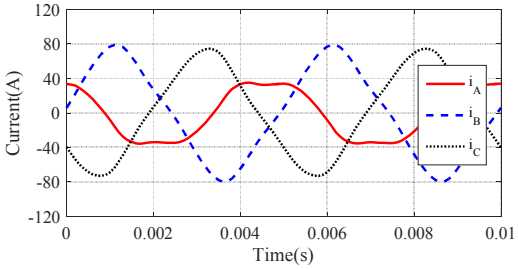

Fig. 19. Short circuit phase currents at 4000rpm.

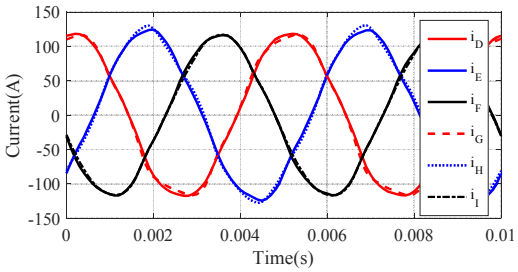

Fig. 20. Healthy phase currents at 4000rpm with set ABC short circuited.

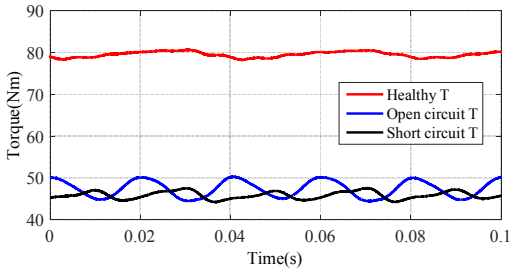

Fig. 21. Torque waveform in healthy, set ABC open circuited, set ABC short circuited condition at 500rpm.

C. Inter-turn Short Circuit Test

Inter-turn short circuit fault is known as the worst fault scenario since only a few turns are involved in the short circuited path. Significantly large current is induced in the fault turns due to the low impedance. The fault is caused by insulation break down and it accounts for a large percentage of faults in electric machines [21, 22]. Thus, inter-turn short circuit fault should be carefully emulated, detected and mitigated. For the machine under study, the inter-turn fault can be alleviated by application of TSC on the faulty 3-phase set to nullify the flux in the fault region. Consequently the fault current is reduced to a much lower and sustainable value. The turn fault may occur in the 6 different coils as shown in Fig. 1. In the event of a turn fault with TSC, the machine operates in an unbalanced manner. It leads to different flux linkages for the 6 coils in this condition, therefore, the fault current after TSC is different if it takes place in different coil locations. The analysis in [14] demonstrates that after TSC in motoring mode the fault current is the largest if a single turn fault occurs in coil B2 while in generating mode the fault current is the highest if the fault takes place in coil A1.

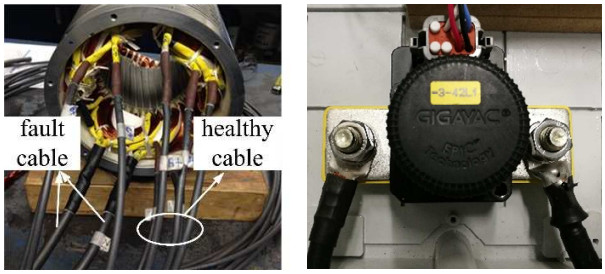

(a) (b)

Fig. 22. Inter-turn short circuit test setup (a) Cable leads (b) Relay.

In order to emulate the worst inter-turn fault case, a single turn tap is brought out in coil B2 of set ABC. Thick cables have been connected to the fault emulation tap to minimize the additional impedance in the short circuited loop as shown in Fig. 22(a). The cable leads are connected to a high current relay as shown in Fig. 22(b) to emulate the inter-turn fault in a controlled manner. It is worth noting that the fault turn is located in coil B2 when the rotor rotates anti-clockwise. However, the fault location is equivalent to that in coil A1 if the rotor rotates clockwise as shown in Fig. 1. Hence, the turn fault could be tested in both coil locations.

1) Without Terminal Short Circuit

First, the inter-turn fault is tested in coil B2 without TSC when the machine rotates anti-clockwise. In order to avoid the damage due to the excessive fault current, the turn fault is tested at 1000rpm when all 3-phase sets are excited with 80A load current by closing the relay for 0.2s. The induced turn fault current reaches 440A as shown in Fig. 23. The turn fault is also tested with variation of load currents from 10A to 80A at 1000rpm in both motoring and generating mode. The measured variation of the RMS fault current with the load currents are plotted in Fig. 24. As can be seen, the RMS fault current under two modes are similar and both increases with load current.

Similar turn fault tests are performed in coil A1 by rotating clockwise. The measured variations of the RMS fault current of both operation modes are plotted in Fig. 24. They also increase with load current however the difference between the motoring and generating mode is slightly larger. It is worth noting that the fault current will be even higher if the load current or speed increases. Therefore, mitigation action is essential to reduce the large fault current in real operation.

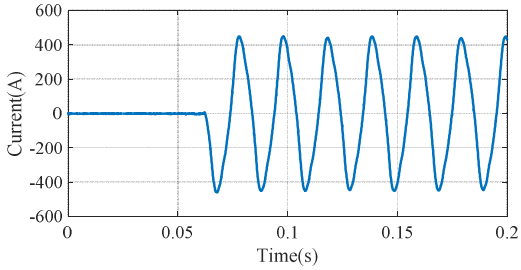

Fig. 23. Turn fault current with 80A load current at 1000rpm.

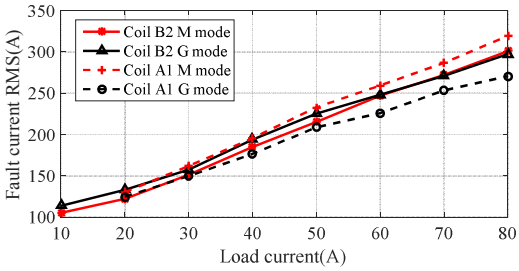

Fig. 24. Turn fault current in coil B2 and A1 variations at 1000rpm in motoring and generating mode.

2) With Terminal Short Circuit

The turn fault is then tested with TSC. Application of TSC can reduce the turn fault current effectively. Thus, the fault can be tested at 4000rpm with 120A current in healthy 3-phase sets. Fig. 25 demonstrates that the fault current has been reduced to about 220A. The phase currents in the faulted 3-phase set are similar to that of one set terminal short circuit as shown in Fig. 19. Meanwhile, the currents of healthy sets are close to that in Fig. 20 which continue to provide torque.

The turn fault with TSC is also tested with variation of currents in the healthy sets from 20A to 120A for emulated turn faults in coil B2 and A1 in both motoring and generating modes, respectively. As will be seen in Fig. 26, the fault current in coil B2 is higher than that in coil A1 in motoring mode while the opposite is true in generation mode. These results are consistent with the findings in [14]. The worst case in motoring mode in terms of continuous operation is determined as a single turn fault in coil B2 when the other healthy 3-phase sets are excited with the rated current. Similar conclusion can be made for generating mode. It should be noted that after TSC the machine can still output about 2/3 of the torque as that of one set short circuit mode as shown in Fig. 17.

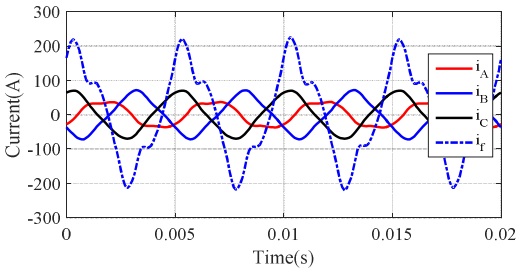

Fig. 25. Turn fault current and phase currents with 120A load current at 4000rpm in motoring mode.

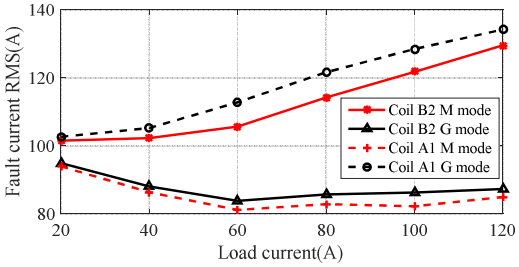

Fig. 26. Turn fault current in coil B2 and A1 variation at 4000rpm in motoring and generating mode after TSC.

3) Combined Test of Fault Injection, Fault Detection and Fault Mitigation

To demonstrate the performance of the fault tolerant drive in response to the worst fault scenario, tests are performed by injecting the single turn short circuit fault when the drive initially operates in healthy condition. In order to mitigate the fault effect, the fault needs to be detected in a timely manner. In this study, the 2nd harmonics in the instantaneous active or reactive powers are employed as fault indicator [23]. In healthy operations, the system is well balanced and the 2nd harmonic in the active and reactive powers in all three 3-phase sets are similar and close to zero. However, this will no longer be true under fault conditions. If the 2nd harmonic in one 3-phase set is significant higher than the reference value under the healthy condition and those of the other two 3-phase sets, a turn fault is indicated and the mitigation action TSC will be taken on the fault set. It is shown that this fault detection technique works well in almost all operating conditions, including during speed and load torque transients by virtue of cross references of the 2nd harmonics in the instantaneous powers in the three 3-phase sets.

A combined test of the fault injection, fault detection and fault mitigation is performed and the results are shown in Fig. 27. Initially the machine is running at 1000rpm with 60A current and a turn fault is triggered by the relay at 0.22s. The fault current increases to 340A immediately. It is seen that the fault is detected within one fundamental cycle (less than 15ms) and the mitigation action is applied. After the TSC, the fault current is effectively reduced to 135A. Meanwhile the operation in the other two healthy 3-phase are virtually unaffected. This is evident from the current waveforms of the other two sets in Fig. 28. Thus, the drive continues to operate albeit its torque capability is reduced.

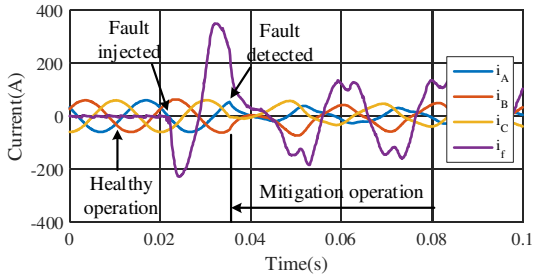

Fig. 27. Combined fault injection, detection and mitigation behavior.

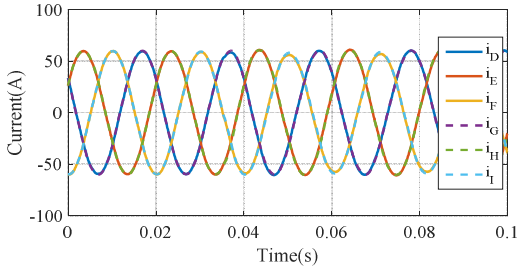

Fig. 28. Phase currents in healthy sets.

4) Thermal Test after Terminal Short Circuit

The fault tolerant capability is further examined by measuring the temperature rise under the worst fault scenario in motoring mode. The test is performed by operating the machine for 2 hours with a single turn fault in coil B2 after application of TSC while the remaining two healthy 3-phase sets are loaded with 120A currents. The recorded temperatures in various parts of the machine are shown in Fig. 29. As will be seen, the

temperatures in the slot and end winding part where the fault turn is located are lower than those in the DEF windings although the fault current is 1.5pu. The temperatures of coil B1 and in the ABC end winding are also lower than those of the DEF windings. Comparing Fig. 16 and Fig. 29, it is observed that the temperatures of the DEF windings are even lower that of the healthy condition. This is because the short circuit phase currents in set ABC are much lower than 120A. Thus, the resultant thermal loading and temperature rises are lower than those under the healthy condition. The tests above confirm that the machine drive can sustain the worst turn fault by TSC with about 1/3 torque reduction without any thermal risk.

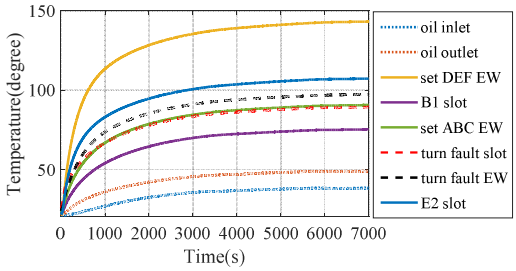

Fig. 29. Thermal test results under single turn fault in coil B2 with 120A at 4000rpm in motoring mode after TSC.

V. DISCUSSIONS

As can be seen, operation of the triple redundant 9-phase machine is symmetrical as the conventional 3-phase machine in healthy conditions. However, the machine will operate in unbalanced manner in fault conditions. The unbalance and resultant coupling between the three 3-phase set can be understood by analyzing the magneto-motive force (MMF) distribution in the air gap.

For the sake of discussion, the ampere-turns of each coil with rated current are denoted as 1 pu. Assuming at time instant $t = 0$, the phase currents are $i_A = i_D = i_G = 1pu$, $i_B = i_C = i_E = i_F = i_H = i_I = -0.5pu$. According to the winding distribution in Fig. 1, the resultant MMF of each 3-phase set can be derived [24] in Fig. 30. It is seen that the MMF produced by each 3-phase set is asymmetrical and it contains an AC component and a pulsating component. The total MMF of the machine is the sum of three MMFs as shown in Fig. 31. It is evident that in healthy operation the total MMF in the air gap is symmetrical while the pulsating component becomes zero. Thus, the machine has the same behavior as the conventional 3-phase machine in healthy conditions. This condition is guaranteed by the fact that the *d-q* axis current commands for the three current controllers are identical. Due to current measurement error and imperfect control, there might be a few percent differences in the actual three 3-phase currents and small mutual coupling may arise. Its effect is minimized by the current feedback control. However, the pulsating component of the combined MMF is no longer zero in a fault condition as shown in Fig. 32 where set ABC is open circuited. Though the currents in the open circuit set is zero, the flux of the remaining healthy sets are asymmetric even with sinusoidal current excitation. This is also true for other fault conditions. The nonzero pulsating component in fault conditions is the main cause of the mutual coupling between the three 3-phase set.

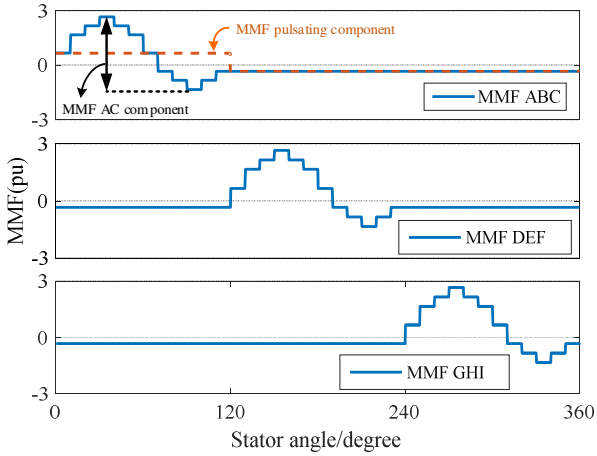

Fig. 30. MMF produced by each 3-phase set.

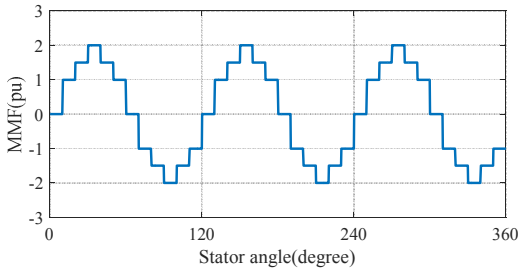

Fig. 31. MMF in healthy condition.

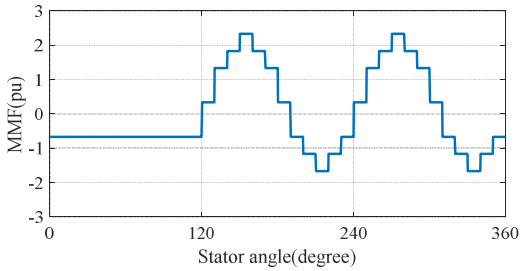

Fig. 32. MMF in open circuit condition.

Simple PI current control with back-emf and conventional decoupling compensation is employed due to the same behavior as the conventional 3-phase machine. However, in fault conditions the nonzero pulsating component in the three 3-phase windings will lead to deterioration of the current control performance. During tests, the 2nd harmonics have been observed in the *dq* voltages as a result of current control action to track the reference. Due to limited current control bandwidth, the currents are distorted as can be seen in Fig. 18. This, in turn, will cause increased torque ripple in fault condition. The current distortion can be reduced by adopting advanced current control strategies such as negative sequence controller or resonant control [25, 26] to suppress the 2nd harmonic. However the resultant improvement in torque quality is not significant because even if in the ideal case of perfectly controlled sinusoidal currents, the torque ripple will still be higher than in the healthy condition since the flux distribution is still asymmetric. Nonetheless, at low speed the torque ripple could be reduced by injecting 2nd harmonics in the *dq* currents as described in [27].

The tests demonstrate that the drive can provide 2/3 of the rated torque continuously while sustaining the worst inter-turn fault with the fault mitigation measure. There are many drive applications in which reduced output power/torque under fault conditions are acceptable. These include EV/HEV tractions, wind power generators, and starter/generator in aircraft. If the full power is required under fault conditions, the inverter and machine can be designed with adequate margin to cope with the requirement at the expense of increased size and weight. In particular, other than removing the whole 3-phase set when one phase is open circuited, the other two phases can be utilized to exploit more torque.

It should be noted that other faults, like mechanical failure, demagnetization fault, may also occur in the machine drive which are not tested. Mechanical failure, including the bearing failure, rotor broken, are usually considered by regular maintenance and replacement. Demagnetization under worst fault conditions has been fully analyzed using the techniques reported in [28, 29]. It has been shown that no demagnetization will take place under any inter-turn short circuit and terminal short circuit conditions. This is because although inter-turn fault current can be many times of the rated, it flows in a few turns, and its overall effect on the magnets which are partly protected by the rotor core is insignificant**.** As mentioned earlier, the PMA SynRM mainly relies on the reluctance torque. Hence the machine drive can still output considerable torque even if an unlikely demagnetization fault occurs.

Cost is an important issue for the 9-phase machine drive implementation when compared with the conventional 3-phase configuration. The cost of the machine is almost the same since only the windings are separated for isolation purpose. The 9-phase drive in Fig. 4 uses three standard 650V, 200A IGBT modules. An equivalently single 3-phase drive will require a single 3-phase module with 600A current capability. The price of IGBT is mainly dependent on the silicon area which is proportional to the current rating. Thus, the cost of the two drives would be quite similar. Additional cost of the triple 3-phase system over the single 3-phase are related to four current sensors and cables. However, these components constitute only a minor part of the total cost of the drive. The volume of the drive is mainly determined by the heat sink. Again, the two drives would require similar size of heat sink. And for the triple 3-phase configuration, the heat can be spread more evenly to the three modules which is the common solution for high power drives [17]. Thus, the power density of the two configurations are also quite close.

VI. CONCLUSION

Comprehensive experimental tests have been performed on a triple redundant 9-phase PMA SynRM drive to assess its performance in healthy conditions and its ability to tolerate various faults, including open circuit, short circuit and inter-turn fault. The test results demonstrate that the machine drive exhibits high performance and excellent fault tolerance over those faults owing to the triple redundant configurations. It has been shown that the worst case fault can be managed by effective fault detection and fault mitigation measure, and the drive is capable of continuous operation with about 2/3 of the output torque without any thermal risk. Further, these tests validate that the proposed fault tolerant drive scheme can be implemented in a simple and cost effective manner. Thus, the machine drive could be a practical candidate for safety critical applications.

REFERENCES

[1] W. Wang, M. Cheng, B. Zhang, Y. Zhu, and S. Ding, "A Fault-Tolerant Permanent-Magnet Traction Module for Subway Applications," *IEEE Transactions on Power Electronics,* vol. 29, pp. 1646-1658, 2014.

[2] O. V. Thorsen and M. Dalva, "A survey of faults on induction motors in offshore oil industry, petrochemical industry, gas terminals and oil refineries," in *Petroleum and Chemical Industry Conference, 1994. Record of Conference Papers., Institute of Electrical and Electronics Engineers Incorporated Industry Applications Society 41st Annual*, 1994, pp. 1-9.

[3] A. H. Bonnett and G. C. Soukup, "Cause and analysis of stator and rotor failures in three-phase squirrel-cage induction motors," *Industry Applications, IEEE Transactions on,* vol. 28, pp. 921-937, 1992.

[4] S. H. Han, T. M. Jahns, M. Aydin, M. K. Guven, and W. L. Soong, "Impact of Maximum Back-EMF Limits on the Performance Characteristics of Interior Permanent Magnet Synchronous Machines," in *Conference Record of the 2006 IEEE Industry Applications Conference Forty-First IAS Annual Meeting*, 2006, pp. 1962-1969.

[5] G. R. Catuogno, G. O. Garcia, and R. Leidhold, "Fault-Tolerant Inverter for Power Flow Control in Variable-Speed Four-Wire Permanent-Magnet Generators," *IEEE Transactions on Industrial Electronics,* vol. 62, pp. 6727-6736, 2015.

[6] N. Bianchi, S. Bolognani, Pre, x, M. D., and E. Fornasiero, "Post-fault operations of five-phase motor using a full-bridge inverter," in *Power Electronics Specialists Conference, 2008. PESC 2008. IEEE*, 2008, pp. 2528-2534.

[7] L. Parsa and H. A. Toliyat, "Fault-Tolerant Interior-Permanent-Magnet Machines for Hybrid Electric Vehicle Applications," *Vehicular Technology, IEEE Transactions on,* vol. 56, pp. 1546-1552, 2007.

[8] B. A. Welchko, T. A. Lipo, T. M. Jahns, and S. E. Schulz, "Fault tolerant three-phase AC motor drive topologies: a comparison of features, cost, and limitations," *Power Electronics, IEEE Transactions on,* vol. 19, pp. 1108-1116, 2004.

[9] B. Mirafzal, "Survey of Fault-Tolerance Techniques for Three-Phase Voltage Source Inverters," *IEEE Transactions on Industrial Electronics,* vol. 61, pp. 5192-5202, 2014.

[10] B. C. Mecrow, A. G. Jack, J. A. Haylock, and J. Coles, "Fault-tolerant permanent magnet machine drives," *Electric Power Applications, IEE Proceedings -,* vol. 143, pp. 437-442, 1996.

[11] T. Raminosoa, C. Gerada, and M. Galea, "Design Considerations for a Fault-Tolerant Flux-Switching Permanent-Magnet Machine," *Industrial Electronics, IEEE Transactions on,* vol. 58, pp. 2818-2825, 2011.

[12] B. Sen and J. Wang, "A fast detection technique for stator inter-turn fault in multi-phase permanent magnet machines using model based approach," in *Power Electronics, Machines and Drives (PEMD 2014), 7th IET International Conference on*, 2014, pp. 1-6.

[13] L. Chong-Zhi, W. L. Soong, B. A. Welchko, and N. Ertugrul, "Uncontrolled generation in interior permanent-magnet Machines," *IEEE Transactions on Industry Applications,* vol. 41, pp. 945-954, 2005.

[14] B. Wang, J. Wang, and A. Griffo, "A Fault Tolerant Machine Drive Based on Permanent Magnet Assisted Synchronous Reluctance Machine " in *Energy Conversion Congress and Exposition (ECCE), 2016 IEEE*, Milwaukee, WI, 2016, pp. 1-8.

[15] L. Alberti and N. Bianchi, "Experimental Tests of Dual Three-Phase Induction Motor Under Faulty Operating Condition," *Industrial Electronics, IEEE Transactions on,* vol. 59, pp. 2041-2048, 2012.

[16] P. Guglielmi, N. G. Giraudo, G. M. Pellegrino, and A. Vagati, "P.M. assisted synchronous reluctance drive for minimal hybrid application," in *Industry Applications Conference, 2004. 39th IAS Annual Meeting. Conference Record of the 2004 IEEE*, 2004, pp. 1-306.

[17] L. Parsa, "On advantages of multi-phase machines," in *Industrial Electronics Society, 2005. IECON 2005. 31st Annual Conference of IEEE*, 2005.

[18] V. I. Patel, "Novel 6-phase fractional slot PM machine for electric vehicle applications," in *the University of Sheffield*, PhD thesis, 2014.
[19] B. Bossmanns and J. F. Tu, "A Power Flow Model for High Speed Motorized Spindles—Heat Generation Characterization," *Journal of Manufacturing Science and Engineering,* vol. 123, pp. 494-505, 2000.
[20] Q. Chen, G. Liu, W. Zhao, L. Sun, M. Shao, and Z. Liu, "Design and Comparison of Two Fault-Tolerant Interior-Permanent-Magnet Motors," *IEEE Transactions on Industrial Electronics,* vol. 61, pp. 6615-6623, 2014.
[21] A. Gandhi, T. Corrigan, and L. Parsa, "Recent Advances in Modeling and Online Detection of Stator Interturn Faults in Electrical Motors," *Industrial Electronics, IEEE Transactions on,* vol. 58, pp. 1564-1575, 2011.
[22] B. Sen and J. Wang, "Stator Interturn Fault Detection in Permanent-Magnet Machines Using PWM Ripple Current Measurement," *IEEE Transactions on Industrial Electronics,* vol. 63, pp. 3148-3157, 2016.
[23] M. Drif and A. J. M. Cardoso, "Stator Fault Diagnostics in Squirrel Cage Three-Phase Induction Motor Drives Using the Instantaneous Active and Reactive Power Signature Analyses," *IEEE Transactions on Industrial Informatics,* vol. 10, pp. 1348-1360, 2014.
[24] J. Faiz, I. T. Ardekanei, and H. A. Toliyat, "An evaluation of inductances of a squirrel-cage induction motor under mixed eccentric conditions," *IEEE Transactions on Energy Conversion,* vol. 18, pp. 252-258, 2003.
[25] S. Hong-Seok and N. Kwanghee, "Dual current control scheme for PWM converter under unbalanced input voltage conditions," *IEEE Transactions on Industrial Electronics,* vol. 46, pp. 953-959, 1999.
[26] A. G. Yepes, F. D. Freijedo, L. Ó, and J. Doval-Gandoy, "Analysis and Design of Resonant Current Controllers for Voltage-Source Converters by Means of Nyquist Diagrams and Sensitivity Function," *IEEE Transactions on Industrial Electronics,* vol. 58, pp. 5231-5250, 2011.
[27] B. Lee, Z. Q. Zhu, and L. R. Huang, "Torque Ripple Reduction for 6-Stator/4-Rotor-Pole Variable Flux Reluctance Machines by Using Harmonic Field Current Injection," *IEEE Transactions on Industry Applications,* vol. 53, pp. 3730-3737, 2017.
[28] S. S. Nair, V. I. Patel, and J. Wang, "Post-Demagnetization Performance Assessment for Interior Permanent Magnet AC Machines," *IEEE Transactions on Magnetics,* vol. 52, pp. 1-10, 2016.
[29] V. I. Patel, J. Wang, and S. S. Nair, "Demagnetization Assessment of Fractional-Slot and Distributed Wound 6-Phase Permanent Magnet Machines," *Magnetics, IEEE Transactions on,* vol. 51, pp. 1-11, 2015.

Bo Wang (M'17) received the B.Eng. and M.Sc. degrees in electrical engineering from Nanjing University of Aeronautics and Astronautics, Nanjing, China, in 2009 and 2012, respectively.

From 2012 to 2014, he served as a senior engineer in the Delta Electronics Co. Ltd. Since 2014, he has been working toward the Ph.D. degree at the Department of Electronic and Electrical Engineering, University of Sheffield, Sheffield, U.K., where he is working as a research associate. His research interests include the permanent magnet machine drives, electric traction and fault tolerant systems.

Jiabin Wang (SM'03) received the B.Eng. and M.Eng. degrees from Jiangsu University, Zhengjiang, China, in 1982 and 1986, respectively, and the Ph.D. degree from the University of East London, London, U.K., in 1996, all in electrical and electronic engineering.

Currently, he is a Professor in Electrical Engineering at the University of Sheffield, Sheffield, U.K. From 1986 to 1991, he was with the Department of Electrical Engineering at Jiangsu University, where he was appointed a Lecturer in 1987 and an Associated Professor in 1990. He was a Postdoctoral Research Associate at the University of Sheffield, Sheffield, U.K., from 1996 to 1997, and a Senior Lecturer at the University of East London from 1998 to 2001. His research interests range from motion control and electromechanical energy conversion to electric drives for applications in automotive, renewable energy, household appliances and aerospace sectors.

He is a fellow of the IET and a senior member of IEEE.

Antonio Griffo (M'13) received the M.Sc. degree in electronic engineering and the Ph.D. degree in electrical engineering from the University of Napoli "Federico II," Naples, Italy, in 2003 and 2007, respectively. From 2007 to 2013, he was a Research Associate with the University of Sheffield, Sheffield, U.K., and the University of Bristol, Bristol, U.K. He is currently a Lecturer with the Department of Electronic and Electrical Engineering, University of Sheffield. His research interests include modeling, control and condition monitoring of electric power systems, power electronics converters, and electrical motor drives, for renewable energy, automotive and aerospace applications.

Bhaskar Sen (M'17) received the B.E. degree from the Delhi College of Engineering, Delhi, India, in 2003, the M.Tech. degree from the Indian Institute of Technology, Kanpur, India, in 2006, both in electrical engineering, and the Ph.D. degree in electrical and electronic engineering from The University of Sheffield, Sheffield, U.K., in 2015. From 2006 to 2011, he was a Research Engineer with GE Global Research, Bangalore, India. From 2015 to 2017, he was a Research Associate at The University of Sheffield. His research interests include electrical machine fault modeling, machine fault detection, and fault-tolerant drives.